Bulletin of the Seismological Society of America, 92, 1, pp. 428–447, February 2002

A Critical Examination of Near-Field Accelerograms from the Sea of Marmara Region Earthquakes

by Sinan Akkar and Polat Gülkan

Abstract In 1999, Turkey was struck by two major earthquakes that occurred 86 days apart on the North Anatolian Fault system. Both earthquakes had right-lateral strike-slip mechanisms with moment magnitudes greater than 7. The number of strong-motion records obtained from the Kocaeli earthquake (17 August 1999, M_w 7.4) was 34. The second event, designated as the Bolu–Düzce earthquake (12 November 1999, M_w 7.2), triggered 20 instruments. Among the records that we have from these earthquakes, seven are from near-source ground-motion data. These records were obtained from the cities of Gebze (GBZ), Yarimca (YPT), İzmit (IZT) (capital city of the province of Kocaeli), Adapazari (SKR) (capital of the province of Sakarya), Düzce (DZC) (shaken strongly in both the events), and Bolu (BOL). In many of these urban centers, extensive structural damage was observed. Although these near-field data have greatly expanded the strike-slip near-source ground-motion database worldwide for $M_w > 7$ earthquakes, they represent a blurred image of the actual severity of the ground motions in the epicentral area because of the sparseness of the national strong-motion network and the unrepresentative geologic conditions at the recording sites. We examine the records to determine whether they provide clues about the extensive damage on the housing stock in the epicentral region. The goal is tackled with earthquake structural engineering criteria in mind, using the drift spectrum as the primary yardstick. There appears to be conflicting evidence that the fault-normal (FN) direction should represent a greater damage-causing potential when this potential is based on ground-story drift spectra. The component with larger ground velocity does correlate better with the component with larger drift demand, but this does not always coincide with the FN direction. The period of the peak velocity pulse matches the structural period where the drift demand is the largest. Further refinements of code requirements that consider this effect are in order.

Introduction

The two earthquakes of the Sea of Marmara region in Turkey during 1999 rank among the largest seismic events that have occurred in the eastern Mediterranean Basin during the last 100 yr. The first of these occurred on 17 August at 3:02 local time and is a multiple rupture event, with M_w 7.4 and M_s 7.8. The second earthquake (M_w 7.2) occurred on 12 November at 6 p.m. Their combined observable fault rupture length was 175 km. We refer to these earthquakes as events 1 and 2, respectively. In terms of their effects (ground deformation patterns, damage, and losses), these earthquakes established new thresholds. Unfortunately, only a patchwork of isolated strong ground motion records was recovered during the mainshock of both the earthquakes. These records are useful, but the instruments lack precise time coordination. Their haphazard locations (instruments are placed in institutional buildings, such as meteorological stations) limited their usefulness. Almost all were stand-alone devices and were triggered on their own, making it difficult to study wave propagation patterns. The mixture of analog and digital sensor outputs introduced another source of dissimilarity into the records that were recovered. The locations of the near-field strong-motion instruments that recorded the 1999 earthquakes are shown in Figure 1. Unfortunately, the sensor in Yalova was being serviced when the earthquake occurred. The names of the affected cities or the location from where the records were taken have been mounted on the space image. The two different lines indicating the approximate location of the observed fault ruptures are shaded differently so that any directivity effects discussed subsequently can be estimated visually. We note that the near-field instruments (indicated by a circle in the figure) were, in many cases, actually placed only a few kilometers away from the actual fault trace.

Gölcük and Yalova, both situated along the southern

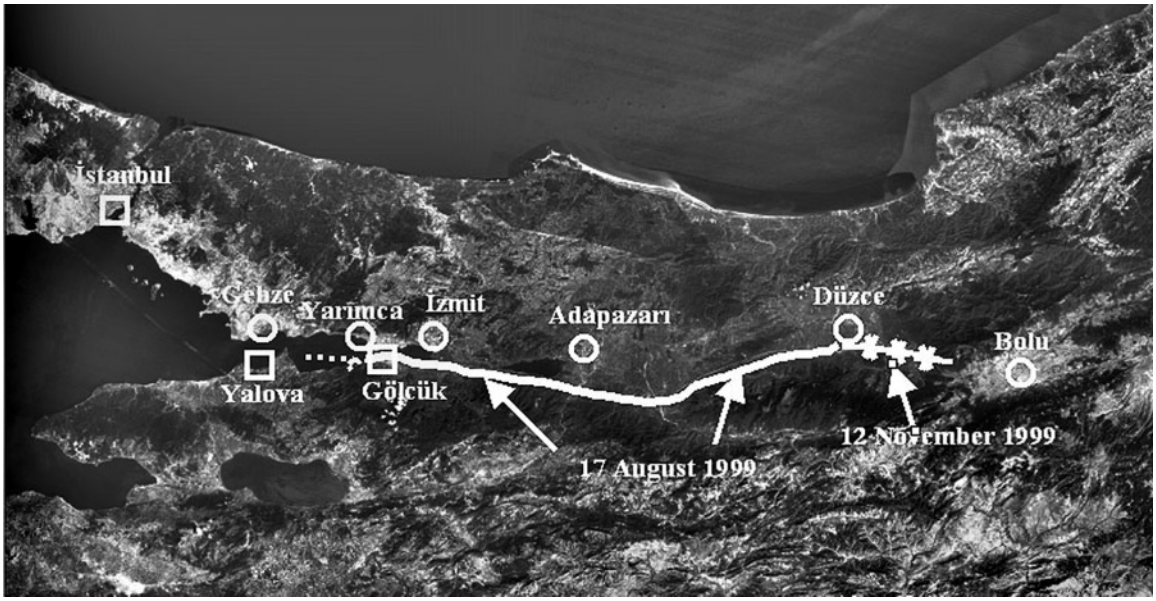

Figure 1. Location of near-field strong-motion instruments that were triggered during the two major earthquakes in Turkey during 1999. The distance from Istanbul to Bolu is 250 km.

coast of the Bay of İzmit, were two of the worst-hit cities. Those and many other smaller settlement centers located along the shore between the cities were the scenes of horrible destruction, but no strong-motion records from these areas exist. For this reason, they are indicated by a rectangle in Figure 1. This unfortunate sparseness has created a void with respect to the question of whether we have an adequate description of how the ground actually moved in the immediate vicinity of the fault rupture. Indirect evidence exists that violent motions must have occurred: parked trucks and passenger busses were overturned at a filling station near İzmit during event 1 and in Kaynasli, a small town 10 km east of Düzce, during event 2. There is other evidence of the extremely strong ground shaking that must have been experienced at close distances to the fault rupture. Widespread damage to buildings, such as seen in Figure 2, in the central part of Gölcük is reminiscent of scenes that resemble bomb-ravaged urban areas during wartime. Such damage must be attributed to many factors, including deficient building practices, but sights such as these are not comparable with, for example, the damage in Erzincan, 700 km east of Ankara, during the M 6.9, 13 March 1992 earthquake, where one component had a peak of 0.5g. Many parts of Gölcük also settled by as much as 1.5 m, a displacement that was accompanied by a 4-m horizontal slip. Such complex patterns of ground deformation are associated with severe demands from structures, but we have no records to confirm this generalization.

Event 1 caused widespread damage along the southern coast of the Bay of İzmit. The epicenter of this earthquake is determined to be directly to the south of İzmit, near a village called Kullar. The rupture then advanced bilaterally, triggering a North Anatolian Fault segment in Arifiye, south of Adapazari, and then, following a step-over, traced a northeast line to Gölyaka, a rural settlement about 15 km southwest of Düzce. Its western propagation bisected Gölcük and smaller settlements in the region. It terminated in the west underwater, probably near the Hersek peninsula (Koçyigit *et al.,* 1999). Event 2 originated at the eastern end of the rupture that was formed by event 1 and propagated to the east, with Bolu in its line of sight. Its occurrence is in agreement with the postulated role of stress transfer and fits the falling domino pattern of earthquake generation along the North Anatolian Fault since 1939 (Stein, 1999). In a strict sense, the BOL record of event 2 is not near field because it was recorded at some 20 km to the nearest fault trace, but it exhibits a strong pulse fling, which is a characteristic feature of such motions. It also contains the largest peak ground acceleration (PGA) value (0.8g) among the seven records that were studied. Other records reportedly obtained from Kaynasli during event 2 were not available to us.

This article examines the available near-source records obtained from these earthquakes in terms of damage-causing potential as understood by earthquake structural engineering. Through an examination of records from the points closest to the affected region, we attempt to reveal if they confirm the type of scene shown in Figure 2. For this purpose, we construct a simple expression for obtaining the drift spectrum, a diagram in which the normalized interstory displacement caused in typical framed structures by a particular ground motion is plotted. We compare the outcome of this exercise with a correlation of the maximum velocity component and examine the effect of the pulse period on elastic interstory displacements in idealized framed structures.

Figure 2. Aerial view of central area of Gölcük. Construction practices limit the drift capacity of typical framed buildings that are usually weaker in the ground story. The result can be structural instability and excessive damage, including collapse.

Evaluation of code provisions that handle the special requirements created by near-field earthquakes is a natural complementary exercise. The database we utilize is composed of seven records from the six cities that are shown in Figure 1. (Düzce had the misfortune of experiencing very strong shaking during both the earthquakes.)

Table 1 summarizes the information relating to the recording stations and sites. In Tables 2 and 3, we summarize the features of the mainshock records for events 1 and 2, respectively. Only the very strong motion parts of some of these traces were used. The complete accelerograms from İzmit (IZT), Gebze (GBZ), Yarimca (YPT), and Adapazari (SKR) contain evidence of waves arriving from subsequent ruptures that are formed during event 1. These effects are not considered in this article, although it is expected that longer duration ground shaking must have exacerbated both structural damage and ground deformation and soil liquefaction observed, particularly in and around Adapazari.

Strong-Motion Networks in Turkey: History and Performance

The national strong-motion accelerograph network in Turkey was initiated in 1973. This network is operated by the General Directorate of Disaster Affairs, part of the Ministry of Public Works and Settlement. Initially, analog acceleration records were installed because they were the technologies available at that time (Inan *et al.,* 1996). During the years that followed, the system was enhanced by the addition of digital instruments. As of May 2001 this system comprised some 140 instruments, which were about evenly divided between analog and digital types. At the expense of introducing interaction effects into the recordings, the instruments are usually placed inside institutional buildings, such as meteorology stations or local ministerial offices for safety, accessibility, phone hookup, and ease of maintenance. None of the stations in the national network has data related to the site geology other than surface observations, hence shear-wave velocity profiles and depths to bedrock are not known accurately. Sometimes, records of instrument characteristics are difficult to obtain. Figure 3 shows their locations. Additional instruments are deployed in Turkey by other agencies and universities. For example, a number of historic religious edifices in Istanbul such as the Saint Sophia Museum and Süleymaniye Mosque have been instrumented with strong-motion sensors on account of their cultural importance. A recently concluded program, managed jointly by the General Directorate of Disaster Affairs and Japan International Cooperation Agency, has established a network in nine provinces in northeastern Turkey between Ankara and Samsun, a city on the Black Sea coast. The purpose of this network is to arrive at quick estimates of losses and casualties if a major earthquake should strike this area. The suspension bridges across the Bosphorus have been the sub-

Table 1
Station Information of the Near-Source Records

Station (Reference)	Elevation (m)	Station Coordinates and Building Description	Recording Site Description*
Sakarya (Adapazari) (SKR)	31	40.737° N–30.384° E Three-story R/C power utility building. Sensor in basement.	The recording station is relatively isolated storage-type building on a gentle hillside. The geological process would be erosion and soil formation of underlying bedrock. Grading has excavated into a hillside, 40 m west of station. Exposed bedrock in hillside is limestone. Structure is too small, and would not have foundation excavated to bedrock-records might show effects of a shallow thin soil layer.
Yarimca (YPT)	10	40.763° N–29.761° E Three-story heavy R/C petrochemical plant administration building.	Local topography is flat, due to being on a river delta with the geological process being dominated by sediment accumulation. Soil appeared to be clay/silt at the surface. Fine-grained materials are expected as the site is relatively far from nearest topography.
İzmit (IZT)	30	40.790° N–29.960° E Single-story meteorological office building.	The recording station occupies inside a switchback in the paved street climbing a steep hillside. The geological process would be erosion and soil formation of underlying bedrock. An old stone fence next to the garden is presumed to be constructed from local rock. It appeared to be made of gray, tightly cement sandstone/limestone mix.
Gebze (GBZ)	30	40.820° N–29.440° E Two-story TÜBITAK research campus building. Ground story sensor.	Local topography has rolling hills, with geological process being soil formation and slow erosion. The foundation of the recording station is almost certainly excavated to rock. Rocky soil near the recording station. Float collected from soil is reddish sandstone.
Düzce (DZC)	110	40.850° N–31.170° E Two-story meteorological office building. Ground-story sensor.	Topography of the area is flat, and soil appeared to be silty-clay at the surface. The active geological process is sediment accumulation, probably in a river floodplain. Clearly in a basin.
Bolu (BOL)	725	40.740° N–31.210° E Sensor in single-story ministry compound building. Adjacent to four-story main block.	The recording station is relatively isolated, adjacent to flat agricultural land. It is near the lowest point in cross section across the valley from north to south. The geological process is one of sediment accumulation, and fine-grain materials are expected as it is relatively far from the nearest significant topography. Soil at the surface is silty-clay. The recording station is situated in a localized pocket of the worst damage in Bolu. It is likely that this station is on the softest, deepest sediments in the Bolu valley.

*Anderson *et al.,* 2001.

ject of health monitoring and have been outfitted with accelerographs operated by the General Directorate of State Highways. The Scientific and Technical Research Establishment of Turkey (TÜBITAK) has funded research programs that have enabled the setting up of small local networks or distributed single instruments designed for specific purposes. Small, purpose-specific clusters of instruments deployed by Middle East Technical University (ODTÜ), Istanbul Technical University (ITÜ), or Bogaziçi University (BÜ) operate as stand-alone systems, mostly in the Istanbul metropolitan area. The General Directorate of State Hydraulic Works (DSI) operates single strong-motion recording systems in and around major dams they have built. Middle East Technical University is in the process of setting up local arrays in the Yalova–Bursa and Aydin–Denizli areas, comprising a total of 20 stations. Bogaziçi University has launched a dense array in the Istanbul area with the purpose of obtaining an early response through shake maps generated from 120 sensors. Clearly, even with these additions, the number of instruments will remain meager for a country with the size and seismicity of Turkey.

All the accelerograms that are listed in Tables 2 and 3 are from the national network, except for the YPT record that has been obtained by a sensor operated by BÜ. The GBZ, IZT, and DZC records were obtained using analog instruments.

General Observations on the Ground Motions

Development of indigenous attenuation relations for ground-motion parameters in Turkey has been hampered by meager data. Traditionally, instrument sensors have been oriented horizontally in the north–south (N–S) and east–west (E–W) directions in Turkey. When values of PGA from Tables 2 and 3 are compared against predictions based on North American or European data, they would seem to be on the low side for these magnitudes and distances. The tables have entries for both these horizontal components, as well as the fault-normal (FN) and fault-parallel (FP) directions as explained in the following sections.

Certainly, peaks of 0.3–0.4*g* from event 1 seem to be inconsistent with the structural performance for most of the

Table 2
17 August 1999 Near-Source Records

Station (Reference)	R_{close}* (km)	Comp	PGA (cm/sec^2)	EPA (cm/sec^2)	PGV (cm/sec)	PGD (cm)	t_{eff} † (sec)	t_{dur} (sec)	T_g‡ (sec)	T_p§ (sec)	PGV/PGA (sec)
		E–W	399.4	313.9	79.8	198.6	12.6		7.2	≈6.0	0.20
Sakarya		N–S	–	–	–	–	–	–	–	–	–
(Adapazari)	3.2	UP	254.1	171.9	42.6	26.8	7.4	65.0	3.8	≈4.0	0.17
(SKR)		FN	–	–	–	–	–	–	–	–	–
		FP	–	–	–	–	–	–	–	–	–
		E–W	226.1	196.2	84.7	167.6	12.3		3.5	≈4.4	0.38
Yarımca		N–S	315.6	195.2	79.6	65.3	12.4		1.4, 3.5–4‖	≈5.0	0.25
(YPT)	3.28	UP	236.2	192.5	33.1	41.2	10.8	30.0	2.8–3.6‖	≈4.0	0.14
		FN	311.5	196.2	78.0	71.1	12.5		1.4, 3.5–4‖	≈5.0	0.25
		FP	222.8	195.2	84.0	165.5	12.2		3.5	≈4.4	0.33
		E–W	222.7	224.7	54.3	129.3	9.9		0.3, 0.6	No pulse	0.24
İzmit;		N–S	163.9	153.0	32.0	47.6	9.2		0.27, 0.5	No pulse	0.20
(IZT)	4.26	UP	146.4	95.2	14.0	11.1	7.7	30.0	2.5, 8	No pulse	0.10
		FN	164.3	155.0	30.9	43.5	9.3		0.27, 0.5	No pulse	0.19
		FP	218.8	223.7	54.8	129.3	9.8		0.3, 0.6	No pulse	0.25
		E–W	140.6	146.2	34.7	103.7	4.8		0.4 6, 6	No pulse	0.25
Gebze		N–S	264.2	179.5	45.6	82.6	6.0		0.55, 6	No pulse	0.17
(GBZ)	7.74	UP	191.7	119.6	12.7	16.9	2.9	30.0	0.5,2.5,6.2	No pulse	0.07
		FN	240.2	201.1	37.0	112.5	5.6		0.5	No pulse	0.15
		FP	136.8	121.6	46.3	97.7	5.3		6	No pulse	0.34
		E–W	375.6	318.8	49.6	108.6	11.0		1.7	≈1.6	0.13
Düzce		N–S	330.5	243.3	60.6	63.8	10.3		0.68, 2.7	No pulse	0.18
(DZC)	17.06	UP	470.9	141.6	21.8	17.0	4.2	27.18	2.8	≈1.6	0.05
		FN	390.1	342.4	67.7	99.0	10.2		1.8	≈1.8	0.17
		FP	267.8	203.1	48.5	51.5	10.8		1.1	No pulse	0.18

*Shortest distance between the observed fault rupture and the recording station.
†Bommer and Pereira (1999).
‡Dominant ground period(s) where the smoothed Fourier amplitude spectrum is maximum.
§Pulse period is defined as the period of largest amplitude pulse-like signal (if it exits) in a velocity trace.
‖Between the period ranges shown, frequency components of the records demonstrate almost an equal amplification.

Table 3
12 November 1999 Near-Source Records

Station (Reference)	R_{close}* (km)	Comp.	PGA (cm/sec^2)	EPA (cm/sec^2)	PGV (cm/ses)	PGD (cm)	t_{eff} † (sec)	t_{dur} (sec)	T_g‡ (sec)	T_p§ (sec)	PGV/PGA (sec)
		E–W	503.3	371.8	86.1	170.1	12.0		0.85	No pulse	0.17
Düzce		N–S	401.8	364.0	65.8	88.0	12.7		0.43, 0.74	No pulse	0.16
(DZC)	8.23	UP	333.3	188.1	28.0	69.0	9.7	25.90	7.8	≈7.4	0.08
		FN	404.2	364.0	62.6	93.2	12.9		0.43, 0.74	No pulse	0.16
		FP	493.2	372.8	84.3	165.3	11.6		0.85	No pulse	0.17
		E–W	805.9	463.0	66.9	21.3	12.5		0.74–1.12‖	≈0.95	0.08
Bolu		N–S	739.5	581.7	58.3	40.3	12.8		0.33, 0.56	No pulse	0.08
(BOL)	20.41	UP	196.2	147.2	24.5	22.1	6.2	50.87	1, 3, 6	≈3.6	0.12
		FN	755.9	423.8	66.9	21.0	12.9		0.74–1.01‖	≈1.05	0.09
		FP	801.6	604.3	56.8	40.8	12.7		0.33, 0.566	No pulse	0.07

*Shortest distance between the observed fault rupture and the recording station.
†Bommer and Pereira (1999).
‡Dominant ground period(s) where the smoothed Fourier amplitude spectrum is maximum.
§Pulse period is defined as the period of largest amplitude pulse-like signal (if it exists) in the velocity trace.
‖Between the period ranges shown, frequency components of the records demonstrate almost an equal amplification.

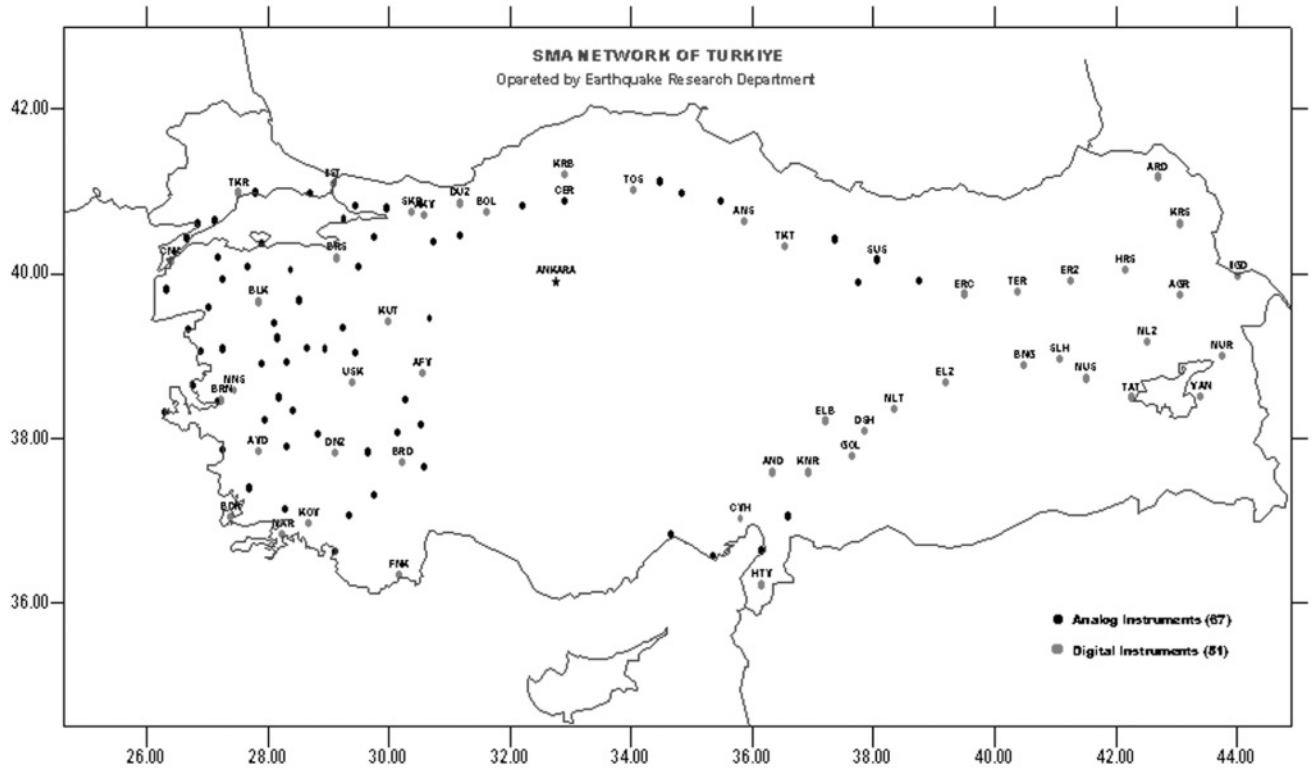

Figure 3. Locations of strong-motion instruments in the National network of Turkey. Nearly all stations are in highest seismic hazard cities, but information about site geology is incomplete.

cities cited in Table 1, but so is the 0.8*g* peak recorded during event 2 in Bolu, where the percentage of collapsed buildings was much less than in İzmit. This conclusion is not applicable to the derived velocity and displacement values. One objective of this study is to test the applicability of the hypothesis that ground motions normal to the direction of fault rupture tend to be more severe than the horizontal component orthogonal to it (Somerville *et al.,* 1997a). For this purpose, the radial line extending from the closest point on the fault rupture to the recording station defines the FN direction. The horizontal component perpendicular to this then becomes the FP component. Because of their azimuths from the observed fault rupture, this definition is nearly coincident with the designation of FN as the geographical north, except for GBZ and BOL. It deviates from true north for DZC for event 1 when the rupture terminated about 17 km southwest of the city. These directions are illustrated in Figure 4 and are the basis of the directions cited in Tables 2 and 3.

The effective duration shown in the tables is based on the bracketed Arias intensity (Bommer and Pereira, 1999). The start of the strong ground shaking is taken as the time when the Arias intensity reaches 0.1 m/sec, and the end is defined as the time when the remaining energy in the entire record equals 0.125 m/sec. According to this definition, any acceleration record whose Arias intensity is less than 0.225 m/sec is not considered as strong ground motion. The dominant ground-motion period, T_g, is defined as the period(s) where the smoothed Fourier amplitude spectrum of the acceleration trace becomes maximum. The term T_p, or pulse period, refers to the period of the velocity pulse with the largest amplitude that constitutes the fling. Where the pulse period can be identified, it is usually similar to T_g. Structural implications of this coincidence are discussed during evaluations of the response and drift spectra.

Derived Velocity and Displacement Records

In deriving the velocity and displacement signals, we used two different procedures: (1) the standard procedure (SCM) applied to 70-mm film analog records of early generation instruments (Trifunac and Lee, 1973) and (2) the alternative procedure (ACM) developed to mimic better the physical environment of near-field earthquakes (Chen, 1995). Integration of two different sets of velocity signals yielded two different generations of displacement signals, but Tables 2 and 3 list ACM values, and only these are exhibited in the subsequent figures. The reason for not utilizing the SCM results for derived quantities was the apparent inconsistency of the permanent offset values with field observations. The ACM is judged to be superior in recovering the long-period components of ground displacements for near-field events. Figures 5–9 display the E–W, N–S, up–down (U–D), FN, and FP components, respectively, of all the seven ground-motion records examined in this article. In each figure, the sequence of the acceleration, velocity, and displace-

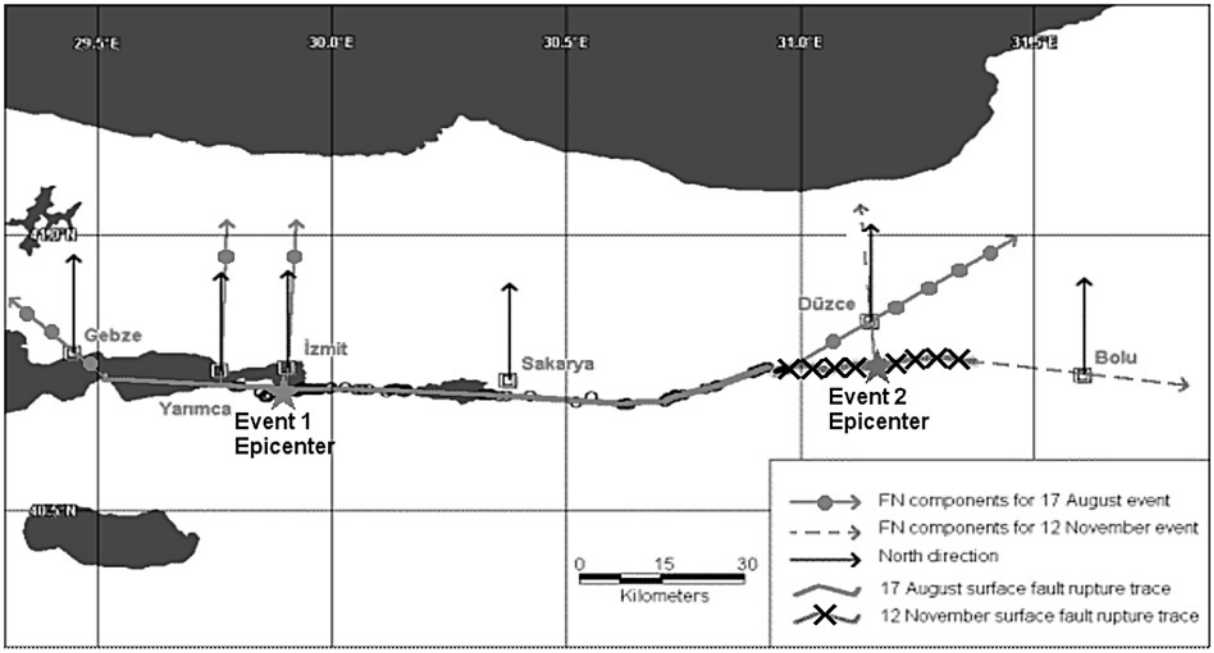

Figure 4. Component directions for the records. Generic definition for FN at each site is according to Somerville *et al.* (1997a).

ment traces are shown. The N–S component of the sensor in SKR malfunctioned during event 1, so this record could not be resolved into other directions.

Most of these traces exhibit typical features from near-field records: large permanent displacement offsets in the strike-parallel direction and large pulselike velocity waveforms, coinciding approximately with the time when the permanent displacements are attained. The inferred rupture propagation direction during event 1 makes all horizontal components in the figures, with the possible exception of IZT, prime candidates for forward directivity effects, and this is supported by the shapes of the corresponding velocity signals. During event 2, the Bolu station appears to have been subjected to a strong velocity pulse, in spite of its relatively large distance of the fault trace. Examination of both these figures and the entries in Tables 2 and 3 show that there appears to be no particular consistency for the larger velocity peak being associated with the FN component. A good example of this is the YPT record, where E–W, N–S, and FP components all have larger peak velocity than the FN component. The IZT and DZC (event 2) records are not affected by forward directivity and have larger velocities either in the E–W or in the FP directions. In contrast, the E–W component of the DZC (event 1) and BOL velocity records displays pulselike segments, as do both components of YPT. These observations are in disagreement with the generalization that the FN is the preferential direction for the occurrence of the pulse (Somerville *et al.,* 1997a). The coherent long-period waves cause the PGV/PGA ratio to become larger, thus making the constant acceleration part of response spectra longer. The structural implications of this observation are discussed separately.

Acceleration and Displacement Spectra

The most widely understood tool for assessing a given motion record in structural engineering is the acceleration spectrum, which in spite of its shortcoming, serves as a device for judging its damage-causing potential. This plot shows the capacity requirement in elastic systems caused by a given ground shaking and is comparable with the unmodified form of the design spectra in codes. The goodness of a given code spectrum may be based on how well it envelops the demands on structural systems created by all conceivable ground motions. Meeting the demands of near-field motions has been incorporated into the Uniform Building Code 1997 (UBC97) requirements (International Conference of Building Officials, 1997) through an upward adjustment of the design spectrum, as schematically described in Figure 10. In contrast, the Turkish Earthquake Code (TEC98) (Turkish Ministry of Public Works and Settlement, 1998), provides no specific requirements for use as a means of guarding against the effects from close events.

The utility of the acceleration spectrum in making assessments related to structural performance during strong ground motions is limited. Figure 11 shows the acceleration spectra for three records from YPT, DZC (event 1), and BOL. In the interest of judging how well two specific structural design codes would have foreseen the envelope of response accelerations at these locations, all diagrams display the code-specified curves in accordance with the UBC97 and TEC98. In terms of general properties, the soil classification pair SD-Z3 (soil sites) in these codes is similar. All records were made on soil sites. At a period range of about 1.0–1.5 sec, which corresponds to the pulse periods of BOL and DZC,

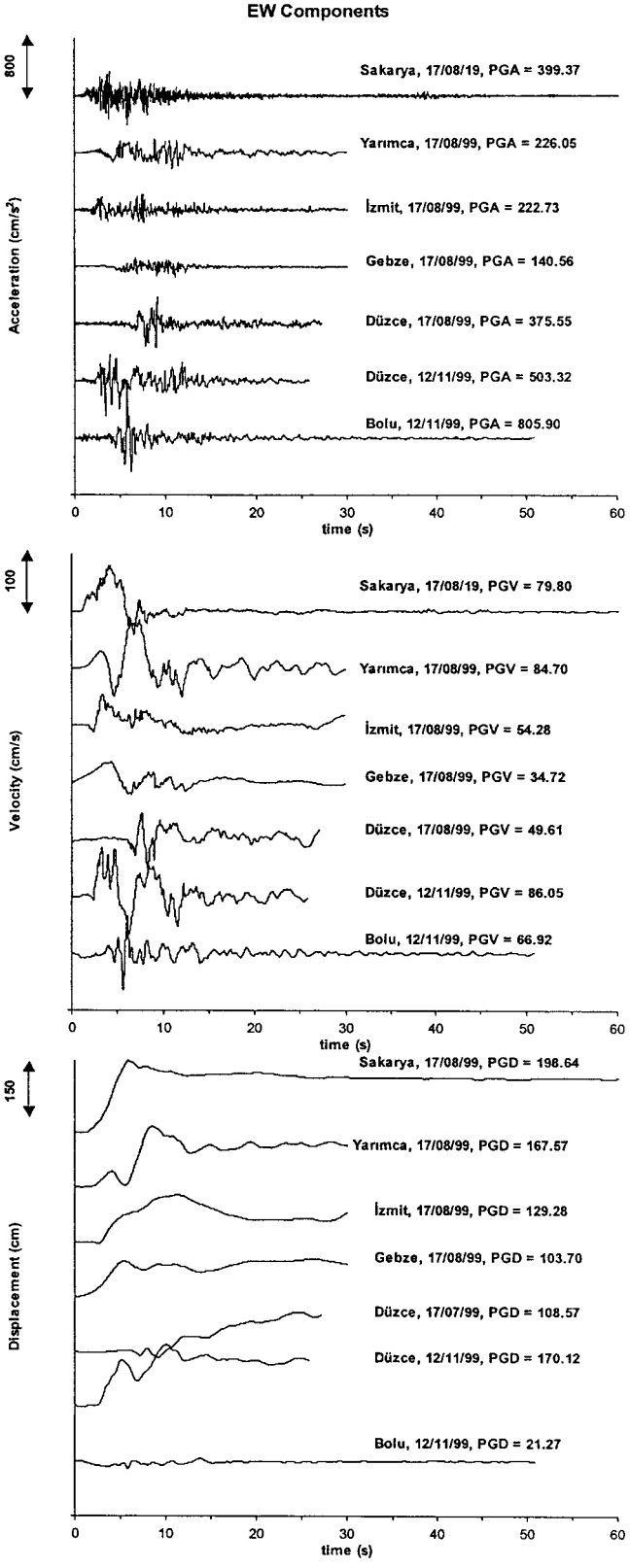

Figure 5. East–west ground-motion signals. For abbreviations of station names see text.

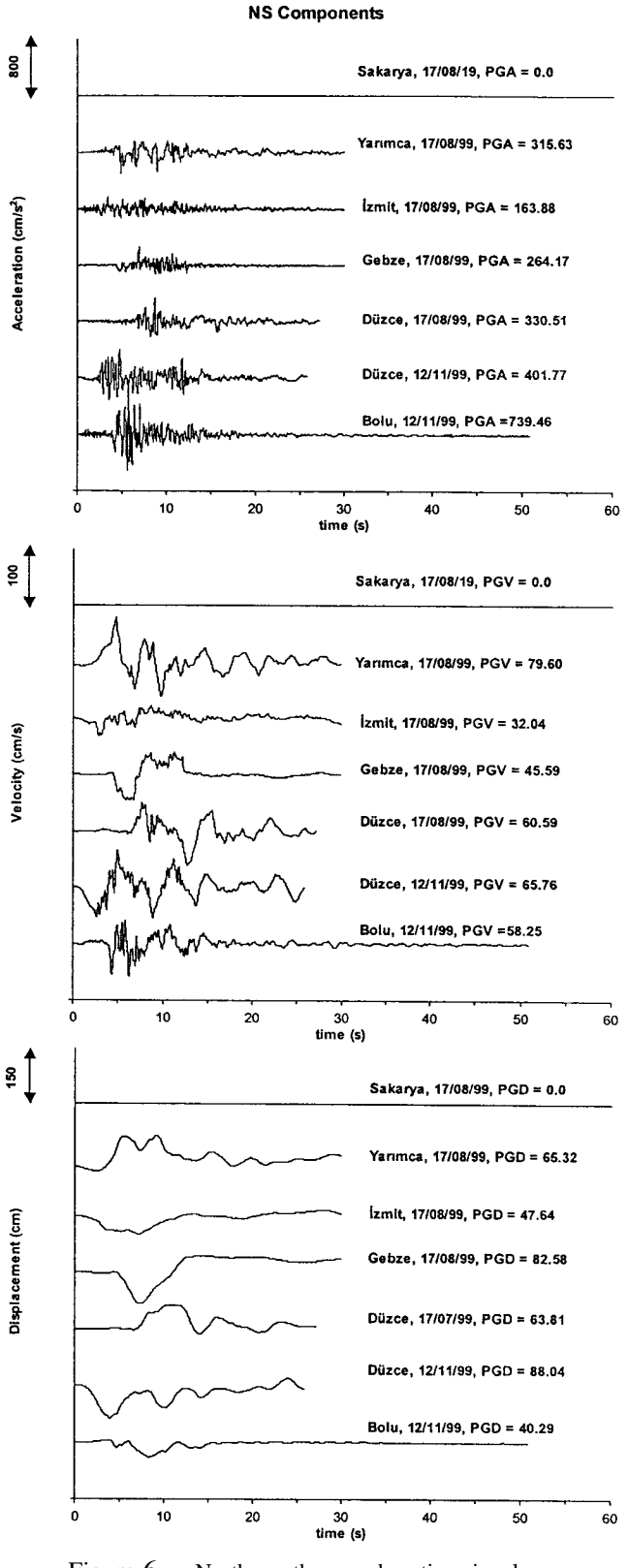

Figure 6. North–south ground-motion signals.

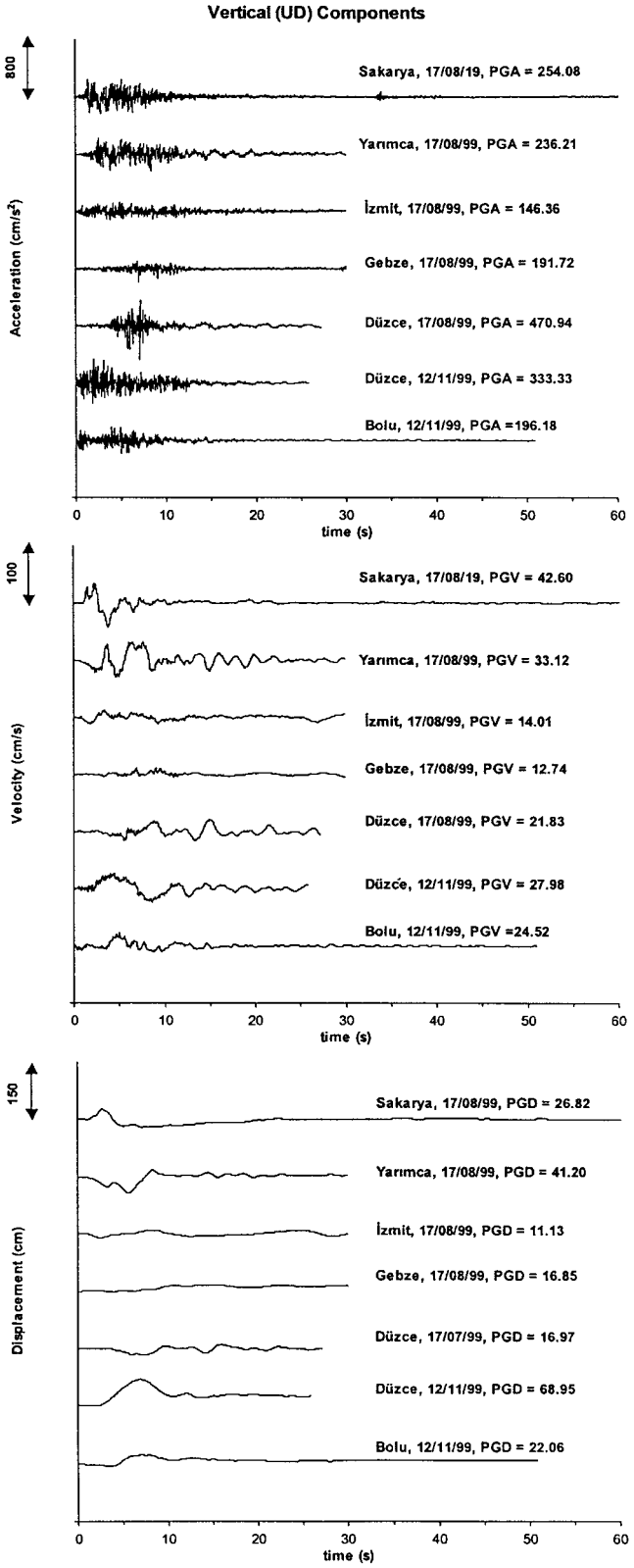

Figure 7. Up–down ground-motion signals.

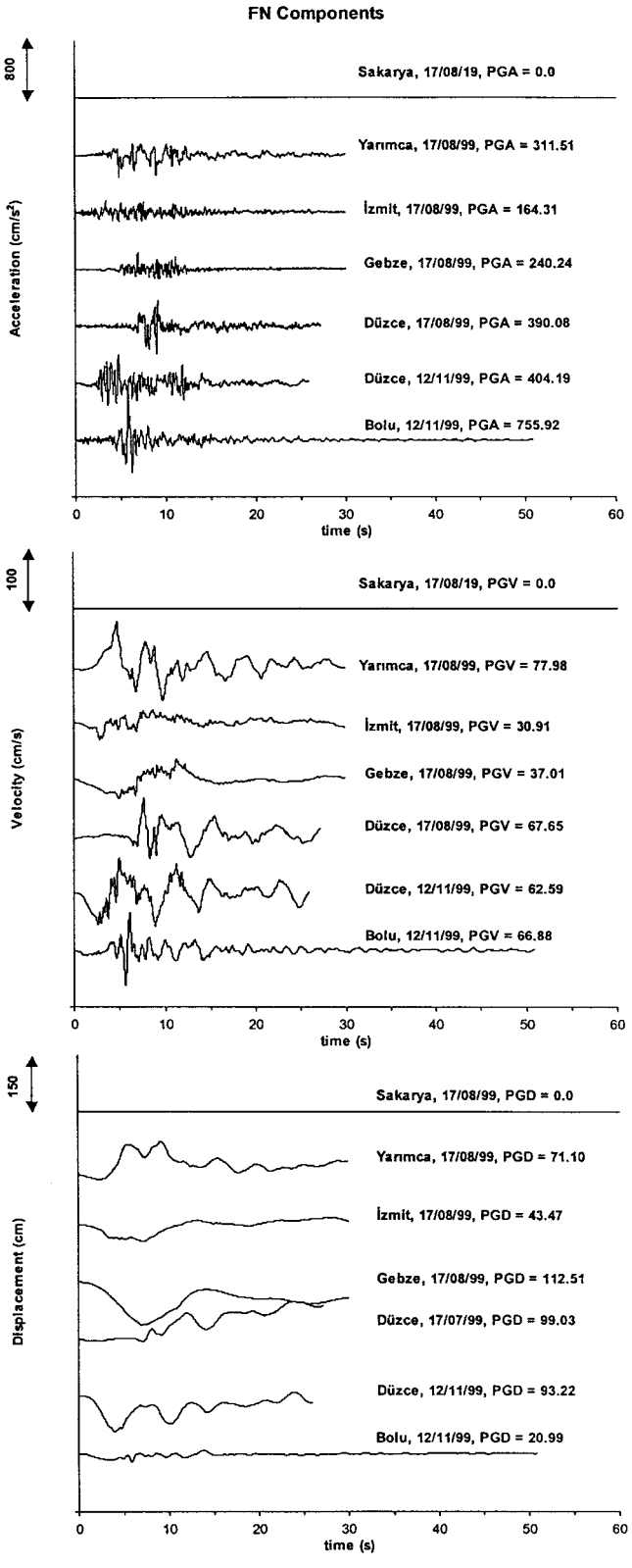

Figure 8. Fault-normal ground-motion signals.

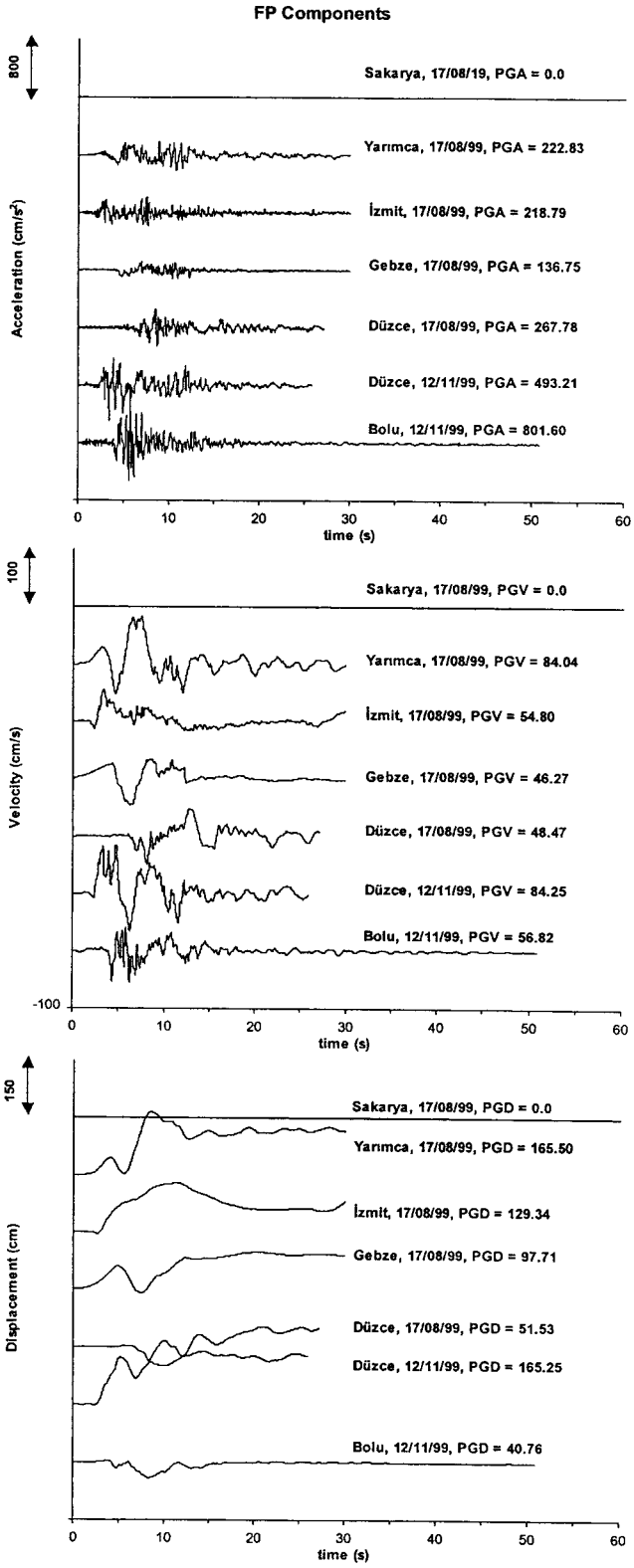

Figure 9. Fault-parallel ground-motion signals.

the capacity demand is considerably in excess of the design spectrum curve. Adjustments required in UBC97 for extending the constant acceleration part follow the trend of the ground motion more closely, but for systems with period in the range of 1 sec or longer, the TEC98 generally falls short. Given the general soft and deep sedimentary soil conditions at DZC, which lies in a river plain, the engineering message conveyed by Figure 11 is that the observed excessive structural damage there might not have been unexpected.

An interesting display of what two successive very strong earthquakes recorded 86 days apart can cause in a city occurred in Düzce. Hundreds of buildings, already weakened during event 1, collapsed, raising the total number to 600. We present the acceleration response spectrum at DZC for event 2 in Figure 12. Upon comparison with the corresponding frame in Figure 11, it is noted that a good deal of similarity exists between the individual plots, except for the emergence of a peak at about $0.8g$ for event 2. It may be argued that the stronger ground shaking during event 2 played a role in shifting the acceleration peak to larger periods. The small building that housed the instrument at Düzce may have modified the free-field motion, but the records are believed to be accurate replications of the actual motions experienced by many structures in the city. This figure demonstrates that similar fault mechanisms and soil conditions cause reasonably similar ground motions at a given site.

A better understanding of the ground motions is possible when their spectral displacement curves are examined because the displacement is a more slowly varying response parameter and is not greatly affected by inelastic structural action. As explained in the following section, spectral displacement can also be utilized for deriving relative interstory drifts. We present the displacement spectra for IZT and BOL in Figure 13. For purposes of comparison, the unreduced spectral displacement derived for the matching soil type, according to UBC97, is mounted on each frame. The figure indicates that in the proximity of pulse periods, the UBC97 significantly underestimates the displacement demand of the E–W and FN components of BOL, although for IZT, where the pulse effect is absent, the actual spectrum falls below the code provisions. This does not agree with field observations at İzmit, where localized pockets in the city and large areas adjacent to the coastal strip in the west suffered heavy structural damage. The rocklike site geology of the recording station masks these effects. A single record on an untypical site helps solely in interpreting the reduced damage at similar sites of the urban area, but its role as a device for postulating why damages were higher elsewhere is not straightforward.

It is necessary to bridge the gap between spectral concepts and structural engineering principles as we attempt to explain why a given ground motion might be more destructive. We utilize displacement-based measures of damage potential in judging how well the specific records made at the locations listed in Table 1 reflect actual experience in their immediate vicinity. Damage occurs when excessive dis-

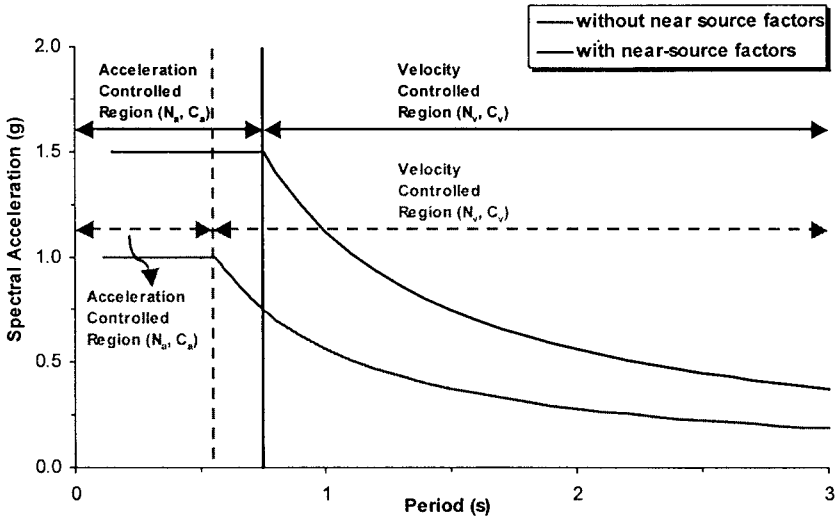

Figure 10. Adjustment of the acceleration spectrum according to UBC97 for near-field earthquakes. The curves correspond to soil profile SC in seismic zone 4. The constant acceleration part of the zone is shifted upward with the use of factors N_a and C_a, and the constant velocity part is similarly modified through N_v and C_v. Both N_a and N_v are dependent on distance to the magnitude of the earthquake on the fault and its slip rate. A distance of less than 2 km and $M > 7$ were assumed here.

placements occur. For idealized framed systems, the drift spectrum is a useful device that quantifies the displacement-causing power a given ground-motion packs.

Drift Spectrum

Examination of the near-source records shown in Figures 5–9 suggests that they contain a number of long-period pulses that, upon integration, translate into longer-period and coherent velocity and displacement pulses with large peaks. In structures subjected to such ground motions, the customary buildup of oscillatory response with several vibration modes dominating the global response may not occur before one of the coherent velocity and displacement pulses propagating through the structure as waves causes a large displacements between successive floors and the associated damage (Iwan, 1997). Drift is the generic term used to define the interstory displacements, traditionally normalized with respect to the height of the story. Emergence of performance-based design criteria favors a renewed expression of structural requirements in terms of permissible displacements. Essentially, the process of structural design in this complementary approach is to determine the displacements in structural components first and then to compare these with allowable limits (Federal Emergency Management Agency, 1997). Displacement limits are defined in terms of the global serviceability criteria that govern postearthquake structural function. Member forces follow after the associated displacements have been found. Consensus is shaping that the Performance Based Seismic Engineering (PBSE) will serve as a rational basis for ensuring the seismic safety of the built environment. Its success will depend on the accuracy of determining displacements in structural assemblies under earthquake effects.

A suitable analytical vehicle utilized to model structural behavior of multistory frames is the shear beam: imagine a large number of rigid laminates, each with mass m connected via laterally flexible links of length h, characterized by their stiffness $12\Sigma EI/h^3$ across any level. Let one end of the assembly be connected to the ground as shown in Figure 14. If this assembly is subjected to a displacement history of $z(t)$ and its time derivative, the velocity history of $v(t)$ at the ground level, then these signals will travel within the beam as damped waves with speed c where

$$c = \sqrt{\frac{12\sum EI}{mh}}. \tag{1}$$

The vibration period, T, is then given by

$$T = \frac{4H}{c}. \tag{2}$$

The equation governing the lateral displacement $u(t)$ is expressed by

$$u(t) = \exp(-\alpha t) f(y \pm ct). \tag{3}$$

The constant α can be related to the viscous damping ratio, ς, as

$$\alpha = \frac{2\pi\varsigma}{T}. \tag{4}$$

The traveling waves will be continuously reflected from the top (free) end and the ground, and the shear deformation $-\partial u/\partial y$ at the base, equivalent to the drift at that level, will be (see Appendix for derivation)

$$\frac{\partial u(T,\varsigma)}{\partial y} = \max_{\forall t} \frac{1}{c}\left| v(t) + \frac{2\pi\varsigma}{T} z(t) \right| + 2 \sum_{n=1}^{N \le 2t/T} (-1)^n \exp(-n\pi\varsigma) \times \left[v\left(t - n\frac{T}{2}\right) + \frac{2\pi\varsigma}{T} z\left(t - n\frac{T}{2}\right) \right]. \tag{5}$$

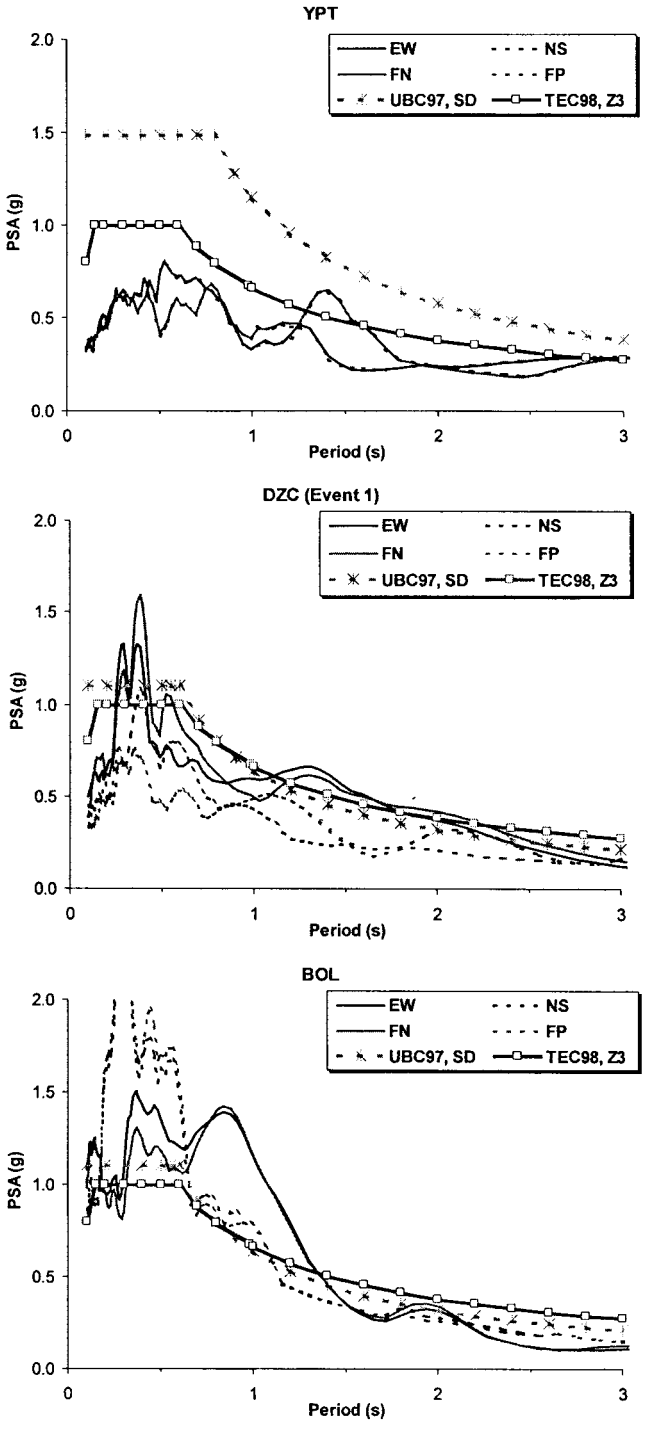

Figure 11. Acceleration spectra for stations YPT, DZC (event 1), and BOL. Unmodified UBC97 and TEC98 design spectra for soil sites are superposed for comparison. The near-field factors for the sites have been calculated for the distances listed in Tables 2 and 3.

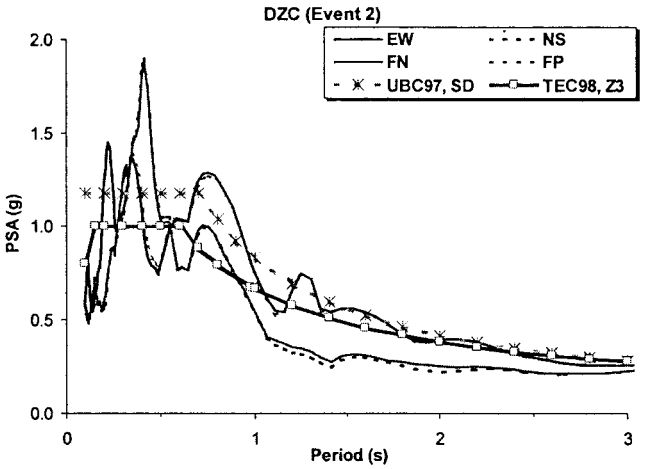

Figure 12. Acceleration spectrum for station DZC (event 2). The near-field factors for DZC have been revised according to the distance listed in Table 3.

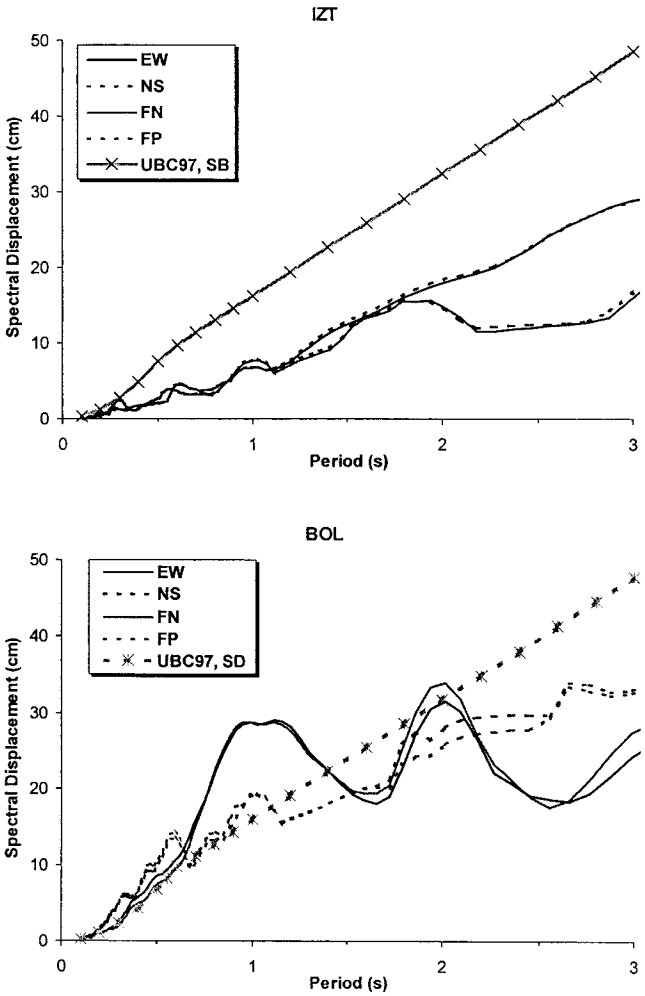

Figure 13. Displacement spectra for stations IZT and BOL. The UBC97 site geology descriptions for soil types SB and SD apply for stations IZT and BOL, respectively.

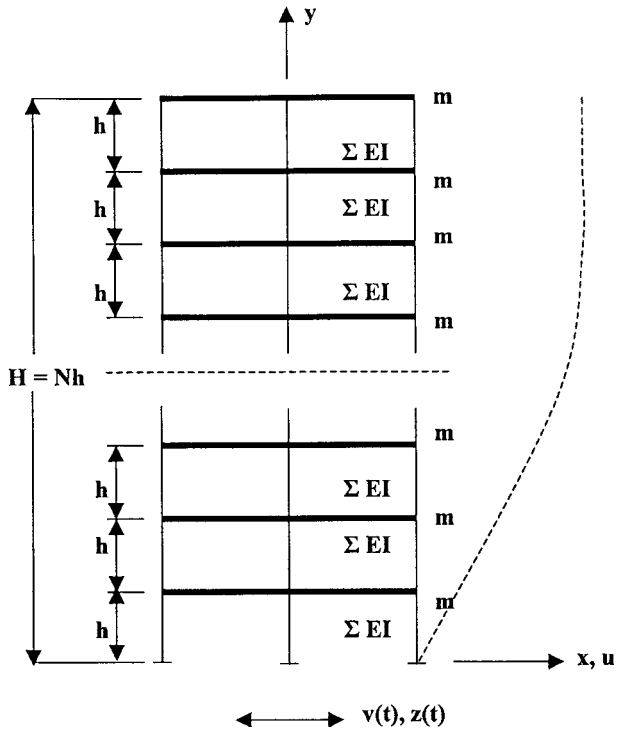

Figure 14. Shear frame idealization. The dashed line describes an arbitrary lateral displacement profile.

In a framed structure, shear deformation is equivalent to the lateral displacement of the first story above ground divided by the height of the ground-story columns or the rotation of the chord connecting the top of ground-level columns to the base. This is called the ground-story drift ratio. The plot of equation (5) as a function of period and damping constitutes the drift spectrum. The period dependence of drift becomes clearer when the expression for c from equation (2) is substituted into equation (5).

The major contribution to drift comes from the ground velocity $v(t)$ and not from $z(t)$ (Akkar and Gülkan, 1999). This confirms that a good measure of the destructive potential of near-field earthquakes is derived from the large velocity peaks they contain. For most structural types, c is typically 100–200 m/sec, so it is conceivable that a single triangular ground displacement pulse with period $2T$, causing a peak velocity in the range of 50 cm/sec, can generate a drift ratio greater than 0.02 (Iwan, 1997). For the quality of materials and workmanship available for reinforced concrete buildings in Turkey, it is likely that columns will develop end yielding at drift ratios below 0.01. The rapid decay of capacity when this action is repeated over several significant cycles can easily cause the types of abject collapse shown in Figure 2.

Figure 15 demonstrates the different characters of near-

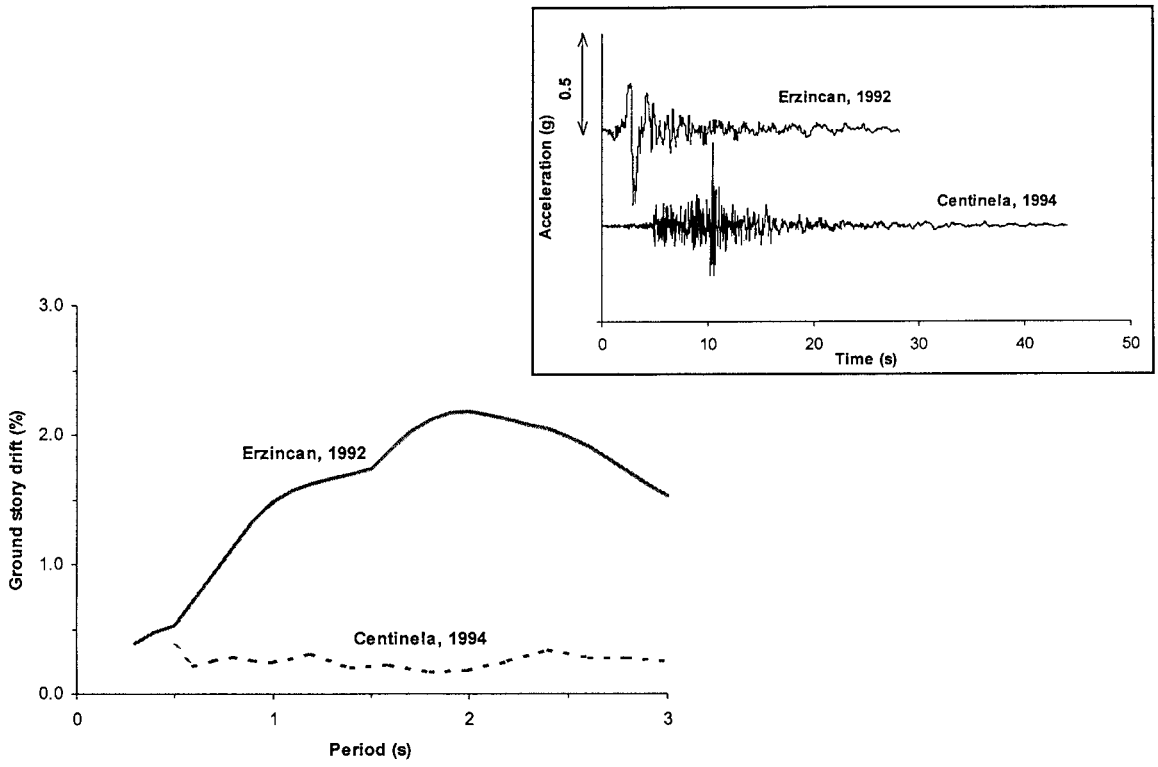

Figure 15. Comparison of base level drift spectra for near-field and far-field earthquakes. The N–S component of the M 6.8 Erzincan earthquake had a peak of 0.402g and was recorded at 2 km. Its PGV was 107.5 cm/sec. The McBride School at Centinela Street S25°E component was recorded during the M 6.7 Northridge earthquake at 25.3 km, and had a PGA of 0.442g and a PGV of 19.9 cm/sec. Site intensities were MSK VIII and MMI VII, respectively.

field ground motions. Two randomly chosen records from earthquakes with similar magnitudes and peak accelerations are considered for the comparison. The records are from the Erzincan (M 6.8) and Northridge (M 6.7) earthquakes. The influence of the coherent large acceleration pulse in the Erzincan record is exhibited through greatly enhanced ground-story drift-ratio demands it causes. This is the most severe demand a near-source ground motion imposes on structural frames.

Alternative Expressions for Drift

Evaluation of the drift expression in equation (5) requires that the time series for the ground velocity and displacement should be at hand. This is not always the case because integration of the acceleration time series is not always a straightforward process. Often, it turns out that nonstandard or unknown procedures have been used for digitization or data reduction from the sensor. Instrument characteristics may not be known accurately. It would be desirable to arrive at the drift spectrum in a way that avoids the use of ground velocity and displacement. In this section we develop a competing simpler replacement for equation (5). In principle, this expression that is applicable to ground-level drift is sufficiently accurate for engineering applications.

Consider the structural frame representation in Figure 14. If this N-story frame consists of members identical in their dynamic properties, then the shear beam expressions for displacement shapes ϕ_n and periods T_n for mode n can be written as

$$\varphi_n(y) = \sin\frac{2n-1}{2}\frac{\pi y}{H}, \tag{6}$$

and

$$T_n = \frac{4N}{2n-1}\left(\frac{m_s}{k_s}\right)^{1/2}, \tag{7}$$

where N is the number of stories, m_s is the story mass, k_s is the story stiffness, and H is the total height of the frame that is equal to Nh.

The assembly shown in Figure 14 serves as a convenient instrument for analysis, also for the case when the base of the structure is subjected to a prescribed ground acceleration $-\ddot{u}_g(t)$. The mode shapes and frequencies derived previously can be utilized for a modal analysis where for each mode an equation of the type

$$u(y,t) = \sum \varphi_n(y) Z_n(t) \tag{8}$$

is used. Then, in mode n with damping ratio ς_n, the equation of motion for the modal amplitude Z_n becomes

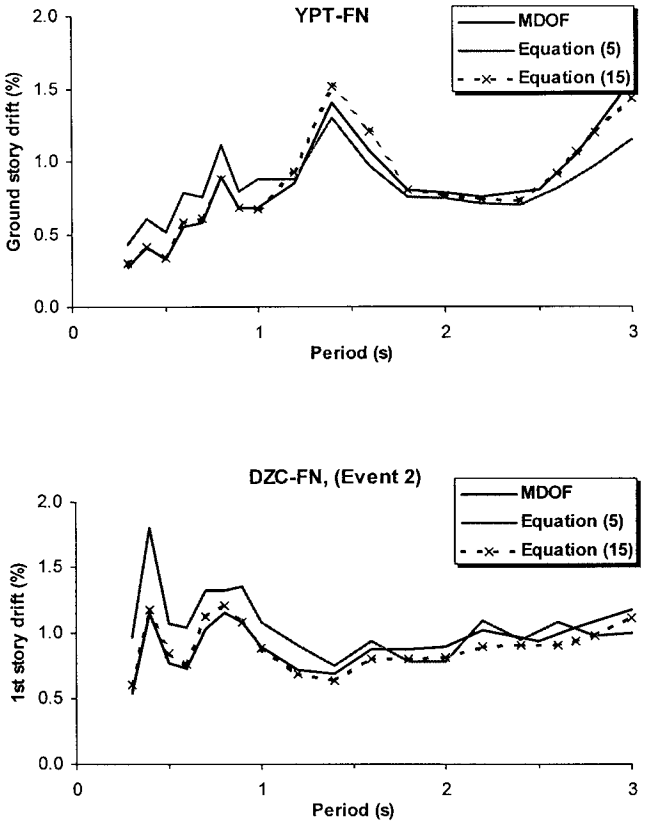

Figure 16. Comparative ground story drift ratio spectra. The structures are 5% damped. The designation MDOF refers to idealized shear frames that serve as checks for the ground-story drifts.

$$\ddot{Z}_n + 2\omega_n\varsigma_n\dot{Z}_n + \omega_n^2 Z_n = \frac{L_n}{M_n}\ddot{u}_g. \tag{9}$$

In equation (9),

$$L_n = \int_0^H \sin\left\{(2n-1)\frac{\pi}{2}\frac{y}{H}\right\}\frac{m}{h}\,dy = \frac{2H}{(2n-1)\pi}\frac{m}{h}, \tag{10}$$

and

$$M_n = \int_0^H \sin^2\left\{(2n-1)\frac{\pi}{2}\frac{y}{H}\right\}\frac{m}{h}\,dy = \frac{H}{2}\frac{m}{h}. \tag{11}$$

Note that $L_1/M_1 = 4/\pi = 1.27$.

We confine our attention to only the first mode because the part of the total mass mobilized in the first mode is approximately 80% of the total mass of the idealized shear frame. In most frames, girders rotate at the column ends, but if the same uniform properties hold along the height and the periods match this generic frame, then the shear frame in Figure 14 would still have the same spectral displacements. Equation (6) states that the largest normalized drift in the fundamental mode occurs at the ground story, where y is equal to h,

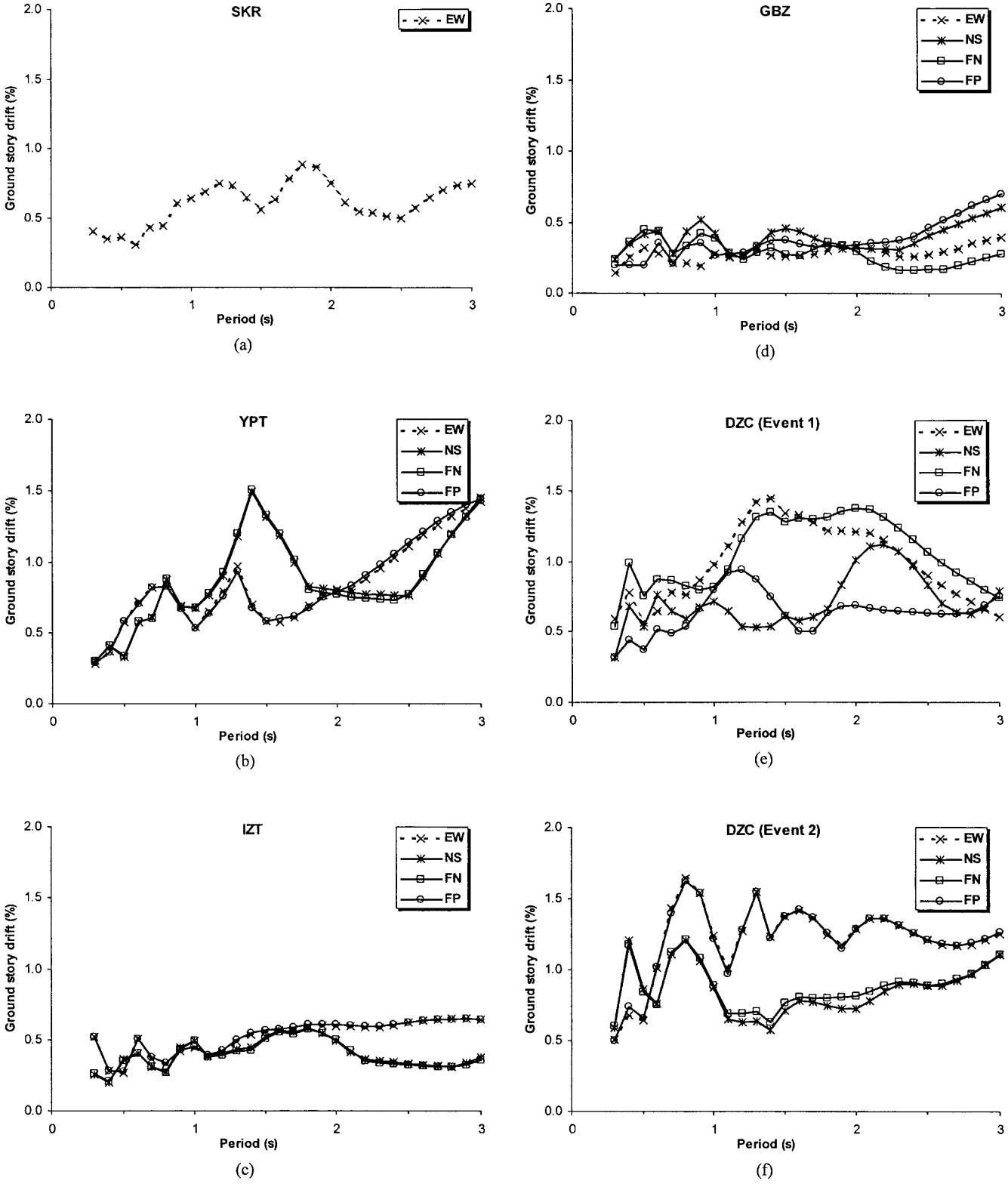

Figure 17. Caption on facing page.

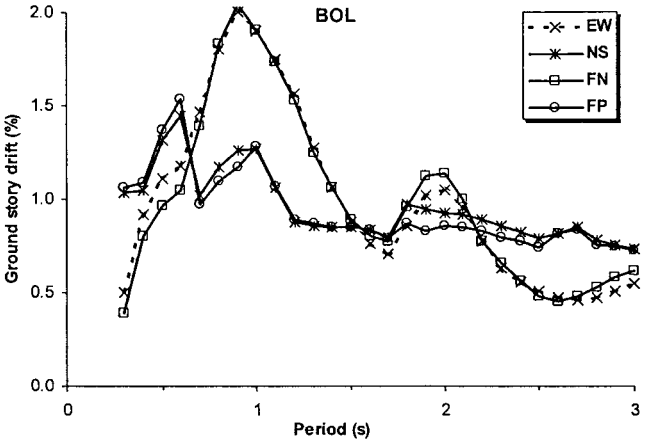

(g)

Figure 17. Comparative drift spectra: events 1 and 2. The curves are computed by using equation (15) for 5% damping. (a) Station SKR; (b) station YPT; (c) station IZT; (d) station GBZ; (e) station DZC, event 1; (f) station DZC, event 2; (g) station BOL.

$$\varphi_1(y) = \sin\frac{\pi}{2N}, \tag{12}$$

and the ground-story drift ratio (GSDR) becomes

$$\text{GSDR} = 1.27\,\frac{\text{SD}}{h}\sin\frac{\pi}{2N}. \tag{13}$$

For a given period and damping ratio, the spectral displacement (SD) can be computed for a given accelerogram. A functional relationship between the remaining parameters of equation (13) and the structural period remains to be established (Gülkan and Sozen, 1999).

In principle, any equation of the type $T = aH^b$ with a and b as regression constants may be used, although for an ideal uniform shear beam, $b = 1$ in view of equation (2). Deviations from the idealized conditions assumed in a shear beam cause this constant to become different from 1. For example, if we take $T = 0.1N = 0.1(H/h)$, for a story height h of 3 m, this is equivalent to $c = 120$ m/sec from the second expression in equation (2). Equating, as an example, the UBC expression

$$T = 0.08H^{3/4} \tag{14}$$

to $T = 4H/c$ we obtain $c = 50H^{1/4}$, which indicates that the apparent shear-wave velocity is a slowly varying function of the building height. Indeed, for $H = 10$ m, $c = 89$ m/sec, and for $H = 100$ m, $c = 158$ m/sec. With this observation, we can now modify equation (13) as follows:

$$\text{GSDR} = 1.27\,\frac{\text{SD}}{h}\sin\frac{2\pi h}{Tc}. \tag{15}$$

The form of equation (15) suggests that variations in the value of c, submerged in the argument of the trigonometric expression, do not play a major role in determining drift.

The analogy with a shear beam is useful for deriving the drift spectrum for a given ground motion, but other models can be utilized. One of these possible approaches is to design a series of simple idealized frames and to vary their stiffness and mass properties systematically so that different periods are obtained. When these frames are subjected to different ground motions, the ground-story displacement divided by its height becomes the drift ratio.

In Figure 16 the comparative ground-story drift spectra for 5% damping are displayed for the FN components of YPT and DZC (event 2), respectively. Qualitatively, and within the degree of accuracy expected from representing complex structural systems by means of simple conceptual models, the three alternative formulations are surprisingly similar. This suggests that the use of the spectral displacements in estimating drift ratios is quite acceptable for the use of structural engineering. In the remainder of this article, we utilize the expression in equation (15) for describing the drift spectra.

Discussion

Different ways might be resorted to for judging how representative the seven records listed in Table 1 were of the general conditions in the affected cities during the two 1999 events in northwestern Turkey. We do this on the basis of their elastic drift spectra. In the interest of uniformity, Figure 17a–g displays their drift spectra for 5% damping for four different directions. Two of these directions correspond to the original sensor orientations and two to the FN or FP components, as they have been defined in Figure 4. The exception to this exercise is of course the SKR record for which only the E–W component is available.

We note that the drift spectrum diagrams for SKR, IZT, and GBZ appear to be no different from the three far-field events shown in Figure 15. These stations are all above rock-like local geology, so the effect of this fact is strikingly evident from frames a, c, and d of Figure 17. The remaining records have peaks reaching orders of magnitude in the range of 1.5–2%, occurring in the proximity of T_p as listed in Tables 2 and 3. Epicentral intensity for event 1 was rated

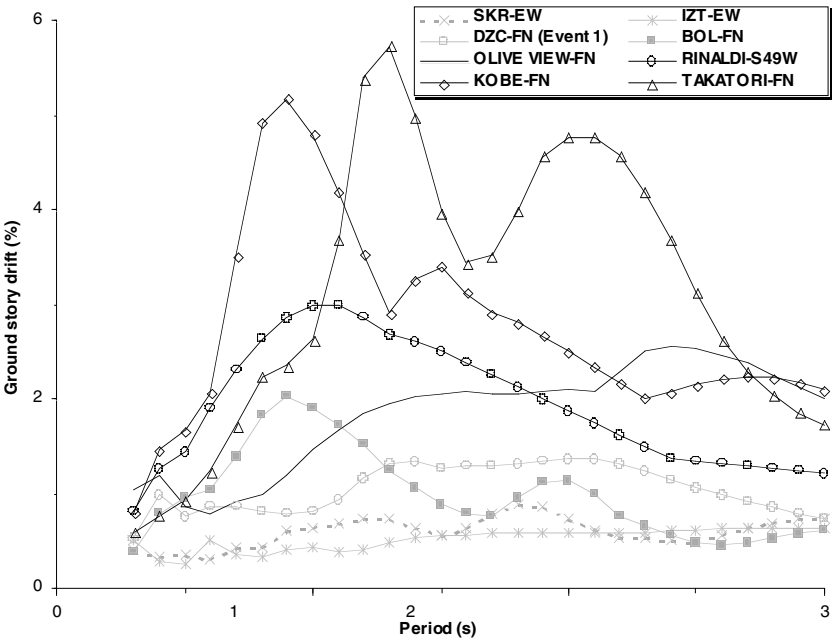

Figure 18. Comparative drift spectra. The drift demands of stations DZC, IZT, and SKR represent the cities that suffered substantial damage during event 1. Station BOL contains the highest drift demand peak among the near-field records of events 1 and 2. The other curves display the near-field drift demand range of the Kobe and Northridge earthquakes for comparison.

as MSK X, although there existed grounds (changes in topography, severe structural damage even in reasonably well constructed facilities, widespread pipe ruptures, etc.) for rating it one-half degree higher in isolated pockets near Gölcük. None of the drift demand curves for either event shown in Figure 18 matches the strongly elongated bias of areas that felt the most damaging ground motions that the isoseismal map in Figure 19 (Özmen, 2000) portrays. For emphasis, Figure 18 includes also curves from the Northridge and Kobe earthquakes (Somerville *et al.,* 1997b) that display the demand range of other near-field records. The severely damaged area had a width of only several kilometers on either side of the fault line. The synoptic picture one has of the distribution of strong ground motion within the epicentral area is shrouded and must be interpreted with caution. In Table 4 we do this by using the device for calculating the area under the drift curves from 0.3 to 3 sec, a range where most structural periods would be represented. Conceptually similar to the Housner spectrum intensity, this measure designated as drift spectrum intensity permits a numerical ranking to be made among the array of components. For completeness, data for the record made at Erzincan on 13 March 1992 and two near-field records from each of the Northridge and the Kobe earthquakes are included in Table 4.

The results, based on records that were available to us, show that observed trends derived from other near-field ground-motion data are not fully supported by the tabulated results. We already mentioned the mismatch of the direction where the maximum ground velocity occurs from the FN orientation. If we accept the premise that drift spectrum intensity is a measure of destructiveness, then our calculations indicate that the maximum ground velocity occurs in the direction where the drift spectrum intensity is also maximum, but this is not necessarily the FN direction. This conclusion is difficult to generalize because when traces from the rock-like local geology at IZT and GBZ are omitted and SKR is excluded because of the single horizontal component it recorded, we are faced with the perplexing reversal of maximum velocity direction between the earlier and subsequent DZC records. During event 1, the FN component has the larger peak velocity of 67.7 cm/sec and drift spectrum intensity of 0.028 sec. But during event 2, it is the FP component with the corresponding values of 84.3 cm/sec and 0.032 sec, respectively. For YPT and BOL, the nearly equal peak velocities in the normal or parallel directions cause a slight increase in the corresponding drift spectrum intensity value, but there exists no discernable difference between them. In a complementary sense, the two atypical near-field records IZT and GBZ yield the largest drift spectrum intensity in the FP components with larger peak velocities, and these occur in the direction of slip. In contrast, all of the remaining motions that are included in Table 4 for comparison yield larger drift intensity spectrum values in the FN direction with the larger peak velocity value. It is puzzling that the near-field records from either of the Turkish events do not seem to fit the expected pattern. For purposes of structural design, our observations, based on Table 4 and Figure 17, may indicate that the building orientation relative to a fault is not as important as the maximum velocity it will experience.

Conclusions

Peak accelerations for most near-source records are not high as expected and seem to become saturated for increasing magnitudes. But their peak velocities and corresponding drift demands are usually considerable, and this has been

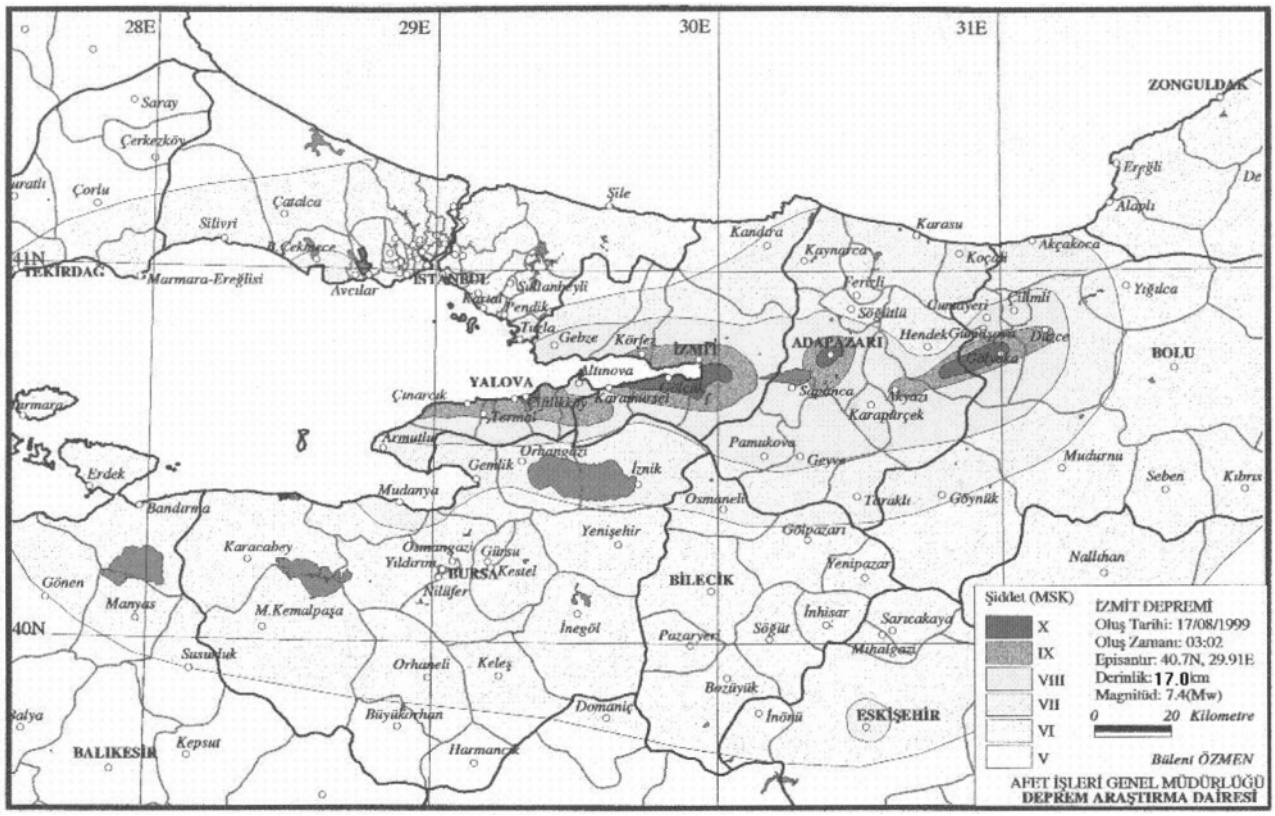

Figure 19. Isoseismal map for event 1 (Özmen, 2000). The darker colors indicate increased MSK scale rating.

Table 4
Comparison of Drift Spectrum Intensities for Near-Field Earthquakes for Structural Damping of 5%

	Drift Spectrum Intensity for Components			
Record	E–W (PGV, cm/sec)	N–S (PGV, cm/sec)	FN (PGV, cm/sec)	FP (PGV, cm/sec)
SKR	0.015 (79.8)	–	–	–
YPT	0.022 (84.7)	0.023 (79.6)	0.023 (78.0)	0.022 (84.0)
IZT	0.013 (54.3)	0.01 (32.0)	0.010 (30.9)	0.014 (54.8)
GBZ	0.007 (37.7)	0.01 (45.6)	0.007 (37.0)	0.010 (46.3)
DZC (event 1)	0.026 (49.6)	0.019 (60.6)	0.028 (67.7)	0.017 (48.5)
DZC (event 2)	0.032 (86.1)	0.022 (65.8)	0.023 (62.6)	0.032 (84.3)
BOL	0.026 (66.9)	0.025 (58.3)	0.026 (66.9)	0.024 (56.8)
Erzincan	0.030 (92.05)	0.041 (107.4)	0.042 (119.2)	0.023 (58.14)
Olive View	–	–	0.048 (122.19)	0.026 (53.19)
Rinaldi recording station	–	–	0.052 (170.32)	0.037 (80.33)
Kobe, JMA	–	–	0.073 (72.35)	0.031 (160.17)
Kobe, Takatori	–	–	0.082 (173.79)	0.040 (63.69)

confirmed by structural damage. Near-field records from the two major earthquakes in the Sea of Marmara region of Turkey have yielded even more modest PGA values than would have been expected, for example from an often-cited source such as Boore *et al.* (1997). The paucity of recording stations has thus made it very difficult to reconstruct a shake map.

It is observed that the pulse period of the records shows a good agreement with the period of the maximum drift demand. The pulse period is approximately the same as the dominant ground period, indicating that it can be a determining parameter for structural response. A closer examination through the use of the drift spectrum of the seven

records from very close distances to the surface rupture of the North Anatolian Fault reveals that they possess puzzling characteristics other than those related to the unrepresentative geological conditions of their sites. The peak ground velocity did not always occur in the FN direction, and the drift spectrum ordinates remained much below other comparable records made both in Turkey and elsewhere. This does not agree at all with the massive destruction of structures along the south coast of the bay of İzmit. The larger ground velocity direction is the critical direction when the drift spectrum intensity used in Table 4 is taken as the measure of destructiveness.

Events with the magnitude similar to that of the two earthquakes examined in this article have probable recurrence periods of several hundreds of years. Because of the lack of densely packed networks of strong-motion transducers, we believe that a rare opportunity was missed in understanding the physics of the faulting and distribution of the ground motion in the epicentral area. We do not have a good understanding of the spatial distribution of the ground shaking on the basis of the seven records analyzed in this article. This underlines the appropriateness of the aphorism that there is no such thing as a redundant strong-motion recorder in a seismic region.

References

Akkar, S., and P. Gülkan (1999). Effect of record processing schemes on damage potential of near-field earthquakes, in *Structural Dynamics-EURODYN '99,* L. Fryba and J. Naprstek (Editors), Vol. 2, A. A. Balkema, 1101–1106, Rotterdam, The Netherlands.

Anderson, J. G., H. Sucuoglu, A. Erberik, T. Yilmaz, E. Inan, E. Durukal, M. Erdik, R. Anooshehpoor, J. N. Brune, and S.-D Ni (2001). Ground motions: implications for seismic hazard analysis, in *1999 Kocaeli, Turkey Earthquake Reconnaissance Report,* T. L. Youd, J.-P. Bardet, and J. D. Bray (Editors), *Earthquake Spectra* **16** (Suppl. A), 113–137.

Bommer, J. J., and A. M. Pereira (1999). The effective duration of earthquake strong motion, *J. Earthquake Eng.* **3,** 127–172.

Boore, D. M., W. B. Joyner, and T. E. Fumal (1997). Equations for estimating horizontal response spectra and peak acceleration from western North American earthquakes: a summary of recent work, *Seism. Res. Lett.* **68,** no. 1, 128–153.

Chen, X. (1995). Near-field ground motion from the Landers earthquake, Report Number. EERL-95-02, Earthquake Engineering Research Laboratory, California Institute of Technology, Pasadena, California.

Federal Emergency Management Agency (1997). NEHRP Guidelines for the Seismic Rehabilitation of Buildings, Federal Emergency Management Agency Publication No. 273, Washington, D.C.

Gülkan, P., and M. A. Sozen (1999). Procedure for determining seismic vulnerability of building structures, *ACI Structural J.* **96,** 336–342.

Inan, E., Z. Çolakoglu, N. Koç, N. Bayülke, and E. Çoruh (1996). Catalog of earthquakes between 1976–1996 with acceleration records, General Directorate of Disaster Affairs, Earthquake Research Division, Ankara.

International Conference of Building Officials (ICBO) (1997). Uniform Building Code, Whittier, California.

Iwan, W. D. (1997). The drift spectrum: a measure of demand for earthquake ground motions, *J. Structural Eng., ASCE* **123,** 397–404.

Koçyiğzzit, A., E. Bozkurt, M. Cihan, A. Özacar, and B. Teksöz (1999). Preliminary geologic report on the August 17, 1999 Gölcük-Arifiye (Northeastern Marmara) Earthquake, Department of Geological Engineering, Middle East Technical University, Ankara.

Özmen, B. (2000). Isoseismal Map, in *August 17, 1999 Bay of İzmit Earthquake Report,* R. Demirtas (Editor), Division of Earthquake Research, General Directorate of Disaster Affairs, Ministry of Public Works and Settlement, 209–221, Ankara (in Turkish).

Somerville, P. G., N. P. Smith, R. W. Graves, and N. A. Abrahamson (1997b). Modification of empirical strong ground motion attenuation relations to include the amplitude and duration effects of rupture directivity, *Seism. Res. Lett.* **68,** 199–222.

Somerville, P. G., N. P. Smith, S. Punyamurthula, and J. Sun (1997a). Development of ground motion time histories for phase 2 of the FEMA/SAC Steel Project, SAC Report Number SAC/BD-97-04.

Stein, R. (1999). The role of stress transfer in earthquake occurrence, *Nature* **402,** no. 9, 605–609.

Trifunac, M. D., and V. Lee (1973). Routine computer processing of strong-motion accelerograms, Report No. EERL-73-03, Earthquake Engineering Research Laboratory, California Institute of Technology, Pasadena, California.

Appendix

Derivation of Equation (5)

With the displacements given by equation (3), the shear deformation of the beam at any elevation y is given by

$$\frac{\partial u}{\partial y} = \exp\left(-\frac{2\pi\varsigma}{T}t\right) f'(y \pm ct). \tag{A1}$$

The velocity at any elevation y is given by

$$\begin{aligned}\frac{\partial u}{\partial t} = \dot{u} &= -\frac{2\pi\varsigma}{T}\exp\left(-\frac{2\pi\varsigma}{T}t\right) f(y \pm ct) \\ &\quad \pm c\exp\left(-\frac{2\pi\varsigma}{T}t\right) f'(y \pm ct) \\ &= -\frac{2\pi\varsigma}{T}u \pm c\frac{\partial u}{\partial y}.\end{aligned} \tag{A2}$$

The expression in equation (A2) for drift can now be revised:

$$\frac{\partial u}{\partial y} = \pm\frac{1}{c}\left(\dot{u} \pm \frac{2\pi\varsigma}{T}u\right). \tag{A3}$$

We are interested in the ground level drift because it is there that the demand is greatest. For $y = 0$, the velocity and displacement of the structure are the same as those of the ground, so we can write

$$\left.\frac{\partial u}{\partial y}\right|_{y=0} = \pm\frac{1}{c}\left\{v(t) + \frac{2\pi\varsigma}{T}z(t)\right\}. \tag{A4}$$

Examining the upward propagation part of the nondispersive wave in the finite length beam expressed in equation (A4), remembering that it is reflected with the same sign from the roof ($y = H$), and with the reversed sign from the ground level ($y = 0$), and taking into account that the duration for a wave to travel to the roof and back is $T/2 = 2H/c$, we can rewrite equation (A4) with the additive effect of all waves that have been reflected until $t = nT/2$ as

$$\frac{\partial u(T,\varsigma)}{\partial y} = \max_{\forall t} \frac{1}{c} \left| v(t) + \frac{2\pi\varsigma}{T} z(t) + 2 \sum_{n=1}^{N \le 2t/T} (-1)^n \exp(-n\pi\varsigma) \times \left[v\left(t - n\frac{T}{2}\right) + \frac{2\pi\varsigma}{T} z\left(t - n\frac{T}{2}\right) \right] \right|. \quad \text{(A5)}$$

This is equation (5).

Department of Civil Engineering and Disaster Management Research Center
Middle East Technical University
Ankara 06531
Turkey
sakkar@metu.edu.tr
a03516@metu.edu.tr

Manuscript received 20 August 2000.